A Non-Reciprocal Filter Using Asymmetrically Transduced Micro-Acoustic Resonators

Mayur Ghatge, *Student Member, IEEE*, Glen Walters, *Student Member, IEEE*, Toshikazu Nishida, *Senior Member, IEEE*, and Roozbeh Tabrizian, *Member, IEEE*

***Abstract*— This letter reports a non-reciprocal filter based on the use of nonlinearities in high quality-factor (*Q*) silicon micro-acoustic resonators with asymmetric piezoelectric transducers. The two-port resonators are created by the integration of 120-nm piezoelectric aluminum nitride and 10-nm ferroelectric hafnium–zirconium-oxide transducers atop of 70-nm single-crystal silicon. The asymmetric electromechanical transduction architecture results in highly contrasted power-handing of the micro-acoustic resonator when excited at different ports, resulting in non-reciprocal transmission response for excitation powers beyond a certain threshold. A proof-of-concept filter at 253 MHz with 0.25% −3-dB bandwidth is implemented through electrical coupling of two asymmetrically transduced resonators with individual *Q* of ∼870. The filter demonstrates a non-reciprocal transmission ratio of ∼16 dB for input power exceeding 5 dBm.**

***Index Terms*— Non-reciprocal filter, nonlinear resonator, hafnium-zirconium-oxide transducer, high-*Q* acoustic resonator.**

I. Introduction

FULL-DUPLEX (FD) integrated RF front-end (RFFE) systems are one of the key enabling modules for realization of the emerging wireless communication protocols (i.e. 5G and beyond). FD RFFE can essentially double the data communication capacity through simultaneous transmission and receive at the same frequency-band and address the ever-growing need for network capacity. Realization of FD RFFE for wireless systems requires integrated non-reciprocal components, such as isolators and circulators, to avoid destructive self-interference between the transmitter (T_x) and receiver (R_x) signals. Such integrated non-reciprocal architectures, however, are not currently available due to the fundamental limitation of current analogue signal processing modules, such as filters and amplifiers that operate inherently on reciprocal physics. Besides FD RFFE, frequency selective limiters (FSL), which are pivotal components in tactical communication systems, require non-reciprocal blockage of in-band signals with large powers that saturate R_x amplifiers. Currently, all FSL technologies rely on ferromagnetic resonators that are very large in size and incompatible with monolithic integration [1]. This leads to the need for research on the development of integrated non-reciprocal architectures based on novel components and systems that break the reciprocity and operate at diverse power ratings. Prominent examples of such architectures are time-varying electronic systems [2]–[4] and active electroacoustic components [5]–[6]. These systems are typically highly complex and impose excessive power-consumption and integration challenges.

In this letter, we introduce a new high quality-factor (Q) micro-acoustic resonator technology that exploits the nonlinear operation regime to enable realization of non-reciprocal RF filters. The presented technology is based on the integration of piezoelectric aluminum nitride (AlN) and ferroelectric hafnium-zirconium-oxide ($Hf_{0.5}Zr_{0.5}O_2$) films on a thin single crystal silicon (SCS) to realize asymmetrically transduced Lamb-wave resonator with non-reciprocal operation.

II. Asymmetrically Transduced Resonators

The non-reciprocal filter presented in this letter are realized through electrical coupling of asymmetrically transduced waveguide-based resonators. Dispersion engineering of the Lamb-waves result in acoustic energy trapping for high-Q waveguide-based resonators [7]. These devices are formed by stacking two piezoelectric transducer films with large thickness variation atop of a thin 70nm SCS layer. The large contrast between the electromechanical transduction efficiency of the two piezoelectric films with large thickness ratio (>10) results in the non-reciprocal power handling of the resonator when excited through different ports. Fig. 1 shows the top view of the asymmetrically transduced resonator. The asymmetric piezoelectric stack is formed by sputtering 120nm piezoelectric AlN film, followed by atomic layer deposition (ALD) of 10nm ferroelectric $Hf_{0.5}Zr_{0.5}O_2$ film. The 10nm ferroelectric $Hf_{0.5}Zr_{0.5}O_2$ is the thinnest ever-reported electromechanical transducer that provides a large piezoelectric coupling when sufficiently polarized [8]. Fig. 2 illustrates the resonator stack, highlighting the diffraction pattern of the orthorhombic $Hf_{0.5}Zr_{0.5}O_2$ layer, sandwiched between the molybdenum (Mo) and TiN electrodes. Fig. 2 (b-inset) shows the ferroelectric hysteresis loop of the TiN/$Hf_{0.5}Zr_{0.5}O_2$/Mo capacitor where a large instantaneous polarization is evident. Application of a sufficiently large DC voltage across the $Hf_{0.5}Zr_{0.5}O_2$ film enables polarization of the transducer to provide linear piezoelectric coupling. The large difference

Manuscript received March 1, 2019; revised March 17, 2019; accepted March 17, 2019. Date of publication March 22, 2019; date of current version April 25, 2019. This work was supported in part by the NSF under Grant ECCS 1610387 and Grant ECCS 1752206. The review of this letter was arranged by Editor S. Pourkamali. *(Corresponding author: Mayur Ghatge.)*

The authors are with the Electrical and Computer Engineering Department, University of Florida, Gainesville, FL 32611 USA (e-mail: ruyam@ufl.edu).

Color versions of one or more of the figures in this letter are available online at http://ieeexplore.ieee.org.

Digital Object Identifier 10.1109/LED.2019.2907089

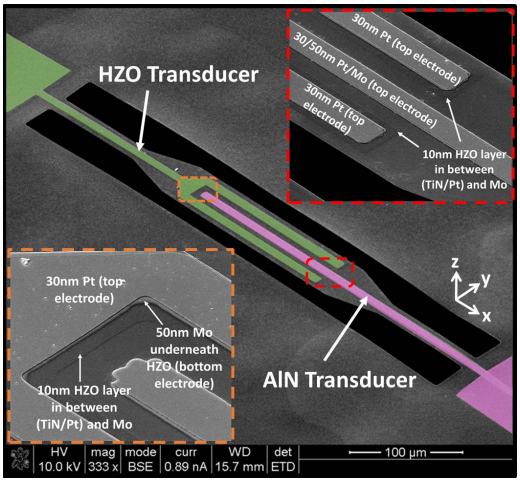

Fig. 1. SEM image of two-port asymmetrically transduced resonator. Port-1 (highlighted in green) is a 10nm ferroelectric $Hf_{0.5}Zr_{0.5}O_2$ film and Port-2 (highlighted in pink) is a 120nm AlN film. The insets highlight the details of $Hf_{0.5}Zr_{0.5}O_2$ transducer stack formed from 10nm ferroelectric film in between 10nm/30nm TiN/Pt on top and 50nm Mo at bottom. AlN transducer is formed from the piezoelectric film with 30nm Pt (top) and 50nm Mo (bottom) electrodes. The device operates based on extensional waves propagating in *Z* direction, with orthogonal displacement in *Y* direction; hence, forming lateral-extensional resonance mode.

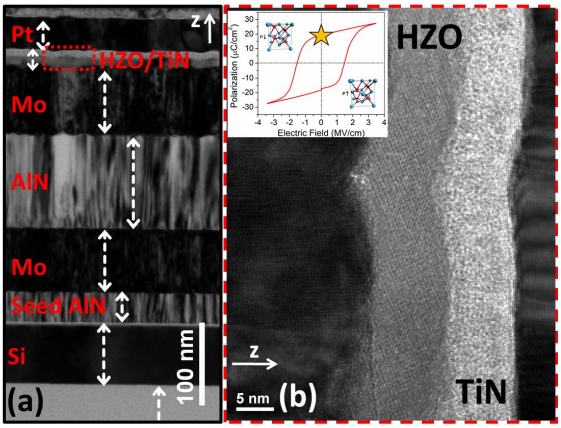

Fig. 2. (a) HR-XTEM image of the resonator stack. (b) Zoomed-in view of the 10nm/10nm $Hf_{0.5}Zr_{0.5}O_2$/TiN layers. The diffraction patters are evident indicating the orthorhombic crystallinity of $Hf_{0.5}Zr_{0.5}O_2$. (inset) Measured hysteresis loop for the 10nm $Hf_{0.5}Zr_{0.5}O_2$. The polarized transducer operates at the starred point yielding a large linear electromechanical coupling.

between the thicknesses of the two transducers (i.e. 120nm AlN vs 10nm $Hf_{0.5}Zr_{0.5}O_2$) results in highly contrasted power handling of the device when excited at different ports. Fig. 3 demonstrates the asymmetric power-handling concept using the Mason waveguide model for the resonator. For a similar electrical input power (i.e. P_{in}), the mechanical energy stored in the resonator can significantly change, depending on the electromechanical excitation port. Specifically, when the resonator is excited at the AlN port, the large $k^2_{eff,AlN}$ can drive the device into mechanical nonlinearities with low input powers. The $k^2_{eff,AlN}$ can be expressed as:

$$k^2_{eff,AlN} \approx k^2_{31,AlN} \cdot \frac{E_{AlN}T_{AlN}}{\sum_n (E_n T_n)} \tag{1}$$

where $k^2_{31,AlN}$ is the transverse coupling coefficient of AlN and E_n and T_n are the Young's modulus and thickness of

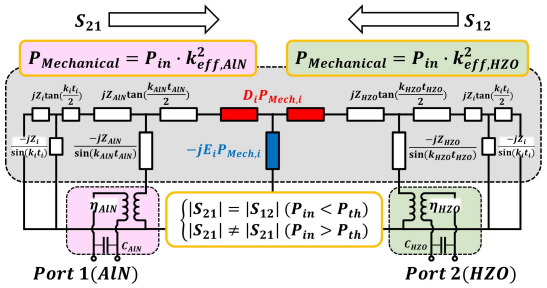

Fig. 3. Mason waveguide model for the resonator with asymmetric transducers. $Z_{AlN/HZO}$, $k_{AlN/HZO}$, $t_{AlN/HZO}$, $C_{AlN/HZO}$ are the acoustic impedance, wavenumber, thickness and static capacitance of the individual transducers and Z_i, k_i, t_i, C_i correspond to other non-piezoelectric materials in the resonator stack. $\eta_{AlN/HZO}$ are transduction efficiencies at two ports and are proportional to $k_{31,AlN/HZO}$ [9]. S_{21} and S_{12} correspond to the mechanical power injected into the resonator when actuated using the AlN and $Hf_{0.5}Zr_{0.5}O_2$ transducers, respectively, using an electric input power P_{in}; Power-sensitive resistive ($D_i P_{Mech,i}$) and reactive ($-jE_i P_{Mech,i}$) components in the model represents the thermal and elastic nonlinear behavior in the i^{th} layer of the resonator.

the corresponding layer in the resonator stack. On the other hand, excitation of the device at the 10nm $Hf_{0.5}Zr_{0.5}O_2$ port with similar input powers does not induce mechanical nonlinearities, due to the significantly smaller $k^2_{eff,HZO}$. The ratio between the electromechanical transduction of the two ports can be expressed through:

$$\frac{k^2_{eff,AlN}}{k^2_{eff,HZO}} = \frac{k^2_{31,AlN}}{A^2 \cdot k^2_{31,HZO}} \cdot \frac{E_{AlN}T_{AlN}}{E_{HZO}T_{HZO}} \tag{2}$$

Here, A is the ratio of effective transduction areas at port-1 and port-2. The large contrast in electromechanical coupling at the two ports, resulting from an order of magnitude difference in the transducer thicknesses, induces a significant change in mechanical energy stored in the resonator when excited with similar input power. While excitation of the resonator at two different ports with sufficiently small input power (P_{in}) results in a reciprocal transmission response, the reciprocity can be directionally broken with the increase in P_{in}. The increase in P_{in}, beyond a certain threshold, drives the resonator into mechanical nonlinearities when using AlN transducer as the excitation port. However, application of the same P_{in} to $Hf_{0.5}Zr_{0.5}O_2$ port does not induce any nonlinearity in resonator operation. In the nonlinear regime, the frequency response of the resonator is substantially distorted resulting in a tremendous increase in the insertion loss. Such distortion can be attributed to the columnar polycrystalline structure of the AlN film that is comprised of dense C-axis oriented grains with loose intergranular bonds. Therefore, excitation of the AlN film with large input powers induces local thermal nonlinearities that essentially distort the resonator frequency response [10]. This behavior is unlike single crystal films or substrates where even large nonlinearities induces a predictable duffing effect in the frequency response of the resonator [11]. The nonlinear operation of the two-port resonator, based on thermal and elastic nonlinearities, are incorporated in Mason waveguide model (Fig. 3) as power-dependent resistive and reactive components.

Considering the operation principle of the non-reciprocal resonator with asymmetric transducers, the dynamic range of

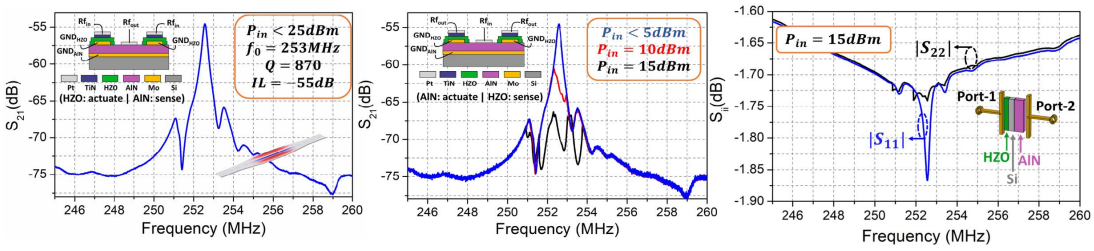

(a) (b) (c)

Fig. 4. (a) Frequency response of individual resonator for different input powers for (a) $Hf_{0.5}Zr_{0.5}O_2$-actuate / AlN-sense (inset shows simulated mode shape of 3rd width-extensional mode) (b) AlN-actuation / $Hf_{0.5}Zr_{0.5}O_2$-sense transduction schemes. (insets-left) show the transduction schemes (c) S_{ii} response of the resonator with different transduction schemes: $Hf_{0.5}Zr_{0.5}O_2$-actuate (S_{11}) and AlN-actuate (S_{22}) for P_{in} = 15dBm.

operation can be defined by:

$$\begin{cases} P_{Mech,forward} = k_{HZO}^2 P_{in} < P_{Mech,threshold} & \text{(3.a)} \\ P_{Mech,\ reverse} = k_{AlN}^2 P_{in} > P_{Mech,threshold} & \text{(3.b)} \end{cases}$$

Here, P_{in} is the input electrical power and $P_{mech,threshold}$ is the threshold mechanical power required to drive the device into nonlinearity. Eq. (3.a) is required to ensure linear operation in forward direction, while Eq. (3.b) is needed to enable signal suppression when operated in backward direction. Eq. (3.a) and (3.b) can be summarized to yield the dynamic range of non-reciprocal operation as:

$$Dynamic\ Range = P_{Mech,\ threshold}\left(\frac{1}{k_{HZO}^2} - \frac{1}{k_{AlN}^2}\right). \quad (4)$$

Considering Eq. (4), the dynamic range can be enhanced by increasing $P_{mech,threshold}$, or increasing the mismatch between electromechanical transduction efficiency at the two ports.

Fig. 4 shows the frequency response of the asymmetrically transduced resonator actuated and sensed at different ports, for different input powers. The 3rd width-extensional bulk acoustic mode is excited at ~253MHz, with a Q of ~870 in both transduction schemes for input powers below 5dBm. However, for the AlN-drive case, the resonator is driven into nonlinear operation with input powers above 5dBm, showing a highly distorted frequency response with an increased insertion loss of ~10dB. On the other hand, in $Hf_{0.5}Zr_{0.5}O_2$-drive scheme, the resonator remains in the linear regime with input powers up to 25dBm, without showing any distortion in response.

III. Non-Reciprocal Electrically Coupled Filters

The asymmetrically transduced resonators are electrically coupled to implement bandpass filters. Opting for a proper coupling architecture, the directional nonlinear response of the individual resonators enables realization of a non-reciprocal filter. In the forward configuration, the excitation is applied to port-1 (i.e. resonator-1 at $Hf_{0.5}Zr_{0.5}O_2$ transducer), and the output is measured at port-2 (i.e. resonator-2 at AlN transducer), resulting in power-insensitive transmission response (i.e. S_{21}). In the backward configuration, the transmission response (i.e. S_{12}) is highly sensitive and gets distorted for input powers above 5dBm. Fig. 5 demonstrates the frequency response of the filter in forward and backward configuration, for different input powers. A non-reciprocal transmission ratio (NTR), i.e. the difference between the insertion losses of forward and backward signal transmission, of ~16dB is achieved for input powers of 5dBm-25dBm. The 20dBm dynamic range of nonreciprocal operation is attributed

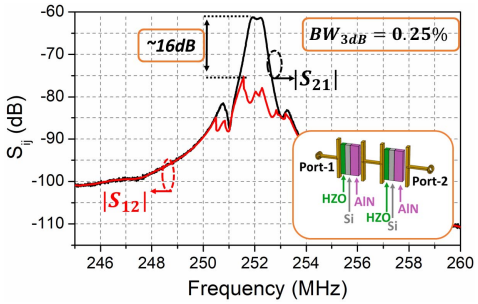

Fig. 5. Measured filter response of the electrically coupled filter with a linear BW_{3dB} of 0.25% and NTR of ~16dB.

to the huge mismatch between electromechanical transduction efficiency at the two ports. This mismatch, however, results in a small $k_{eff,overall}^2$ of the resonator, which limits the maximum attainable bandwidth (i.e. 0.25%) and increases the insertion loss (i.e. −60dB) of the electrically coupled filter. These characteristics can be significantly improved by opting for thicker transducer films with larger piezoelectric coupling coefficients, larger device area, and removing electromechanically passive layers (i.e. Si and TiN) out of the resonator stack. Alternatively, the dynamic range of operation can be increased by opting for $P_{mech,threshold}$ enhancement, while reducing the electromechanical coupling efficiency mismatch at the two ports; thus, improving $k_{eff,overall}^2$.

IV. Conclusion

This letter introduces an asymmetrically transduced micro-acoustic resonator that enables realization of non-reciprocal filters. The resonators are formed from integration of 120nm piezoelectric AlN and 10nm ferroelectric $Hf_{0.5}Zr_{0.5}O_2$ transducers. The significant difference in transducer thicknesses results in a large contrast in resonator power handling when excited at different electromechanical transduction ports. The large distortion of the resonator frequency response in the nonlinear operation regime is used to implement a non-reciprocal filter for input powers beyond 5dBm. The filter is created from electrical coupling of identical asymmetrically transduced resonators at dissimilar transduction ports to create a directional transmission response. Proof of concept resonators at ~253 MHz, with Q of ~870, is demonstrated and used to implemented filters with 0.25% bandwidth. A non-reciprocal transmission ratio of ~16dB is measured for input powers >5dBm. This conceptual demonstration identifies a new approach for realization of non-reciprocal filters to enable 5G full-duplex wireless systems and frequency selective limiters.

References

[1] M. A. Morton and G. Sollner, "Frequency selective limiter," U.S. Patent 9 711 839, Jul. 18, 2017.

[2] J. Zhou, N. Reiskarimian, and H. Krishnaswamy, "9.8 Receiver with integrated magnetic-free N-path-filter-based non-reciprocal circulator and baseband self-interference cancellation for full-duplex wireless," in *IEEE Int. Solid-State Circuits Conf. (ISSCC) Dig. Tech. Papers*, Jan./Feb. 2016, pp. 178–180. doi: 10.1109/ISSCC.2016.7417965.

[3] Y. Yu, G. Michetti, A. Kord, D. Sounas, F. V. Pop, P. Kulik, M. Pirro, Z. Qian, A. Alu, and M. Rinaldi, "Magnetic-free radio frequency circulator based on spatiotemporal commutation of MEMS resonators," in *Proc. IEEE Micro Electro Mech. Syst. (MEMS)*, Jan. 2018, pp. 154–157. doi: 10.1109/MEMSYS.2018.8346507.

[4] M. M. Torunbalci, T. J. Odelberg, S. Sridaran, R. C. Ruby, and S. A. Bhave, "An FBAR circulator," *IEEE Microw. Wireless Compon. Lett.*, vol. 28, no. 5, pp. 395–397, May 2018. doi: 10.1109/LMWC.2018.2815271.

[5] H. Zhu and M. Rais-Zadeh, "Non-reciprocal acoustic transmission in a GaN delay line using the acoustoelectric effect," *IEEE Electron Device Lett.*, vol. 38, no. 6, pp. 802–805, Jun. 2017. doi: 10.1109/LED.2017.2700013.

[6] S. Ghosh, T. Hancock, M. Storey, L. Parameswaran, M. Geis, R. Ralston, and D. Weinstein, "Nonreciprocal acoustoelectric interaction of surface waves and fluorine plasma-treated AlGan/GaN 2DEG," in *Proc. 19th Int. Conf. Solid-State Sens., Actuators Microsyst. (TRANSDUCERS)*, 2017, pp. 1939–1942. doi: 10.1109/TRANSDUCERS.2017.7994448.

[7] M. Ghatge, V. Felmetsger, and R. Tabrizian, "High $k_t{}^2Q$ waveguide-based ScAlN-on-Si UHF and SHF resonators," in *Proc. IEEE Int. Freq. Control Symp. (IFCS)*, May 2018, pp. 1–4. doi: 10.1109/FCS.2018.8597447.

[8] M. Ghatge, G. Walters, T. Nishida, and R. Tabrizian, "A nano-mechanical resonator with 10 nm hafnium-zirconium oxide ferroelectric transducer," in *IEDM Tech. Dig.*, Dec. 2018, pp. 4–6. doi: 10.1109/IEDM.2018.8614633.

[9] S. Sherrit, S. P. Leary, B. P. Dolgin, and Y. Bar-Cohen, "Comparison of the Mason and KLM equivalent circuits for piezoelectric resonators in the thickness mode," in *Proc. IEEE Ultrason. Symp. Int. Symp.*, vol. 2, Oct. 1999. pp. 921–926. IEEE. doi: 10.1109/ULTSYM.1999.849139.

[10] M. Ghatge and R. Tabrizian, "The effect of elastic anharmonicity on the nonlinear behavior of waveguide-based AlN resonator," in *Proc. Joint Conf. Eur. Freq. Time Forum IEEE Int. Freq. Control Symp. (EFTF/IFCS)*, Jul. 2017, pp. 20–21. doi: 10.1109/FCS.2017.8088788.

[11] M. Ghatge, P. Karri, and R. Tabrizian, "Power-insensitive silicon crystal-cut for amplitude-stable frequency synthesis," in *Proc. IEEE 30th Int. Conf. Micro Electro Mech. Syst. (MEMS)*, Jan. 2017, pp. 76–79. doi: 10.1109/MEMSYS.2017.7863343.